Structures of the karyopherins Kap121p and Kap60p bound to the nuclear pore targeting domain of the SUMO protease Ulp1p

Hidemi Hirano,[1,2] Junya Kobayashi,[1] and Yoshiyuki Matsuura[1,2,*]

[1]Division of Biological Science, and [2]Structural Biology Research Center, Graduate School of Science, Nagoya University, Japan.

* Correspondence:

Tel: +81 52 789 2585 Fax: +81 52 789 2989

E-mail: matsuura.yoshiyuki@d.mbox.nagoya-u.ac.jp

Abstract

The budding yeast SUMO protease Ulp1p catalyzes both processing of newly synthesized SUMO to its mature form and deconjugation of SUMO from target proteins, thereby regulating a wide range of cellular processes including cell division, DNA repair, DNA replication, transcription, and mRNA quality control. Ulp1p is localized primarily at the nuclear pore complex (NPC) through interactions involving the karyopherins Kap121p and Kap95p-Kap60p heterodimer, and a subset of nuclear pore-associated proteins. The sequestration of Ulp1p at the nuclear periphery is crucial for proper control of protein desumoylation. To gain insights into the role of the karyopherins in regulating the localization of Ulp1p, we have determined the crystal structures of Kap121p and Kap60p bound to the N-terminal noncatalytic domain of Ulp1p that is necessary and sufficient for NPC targeting. Contrary to a previous proposal that Ulp1p is tethered to the transport channel of the NPC through unconventional interactions with the karyopherins, our structures reveal that Ulp1p has canonical nuclear localization signals (NLSs): (1) an isoleucine-lysine (IK)-NLS (residues 51-55) that binds to the NLS-binding site of Kap121p, and (2) a classical bipartite NLS (residues 154-172) that binds to the major- and minor-NLS binding sites of Kap60p. Ulp1p also binds Kap95p directly and the Ulp1p-Kap95p binding is enhanced by the importin-β-binding (IBB) domain of Kap60p. GTP-bound Gsp1p (the yeast Ran orthologue) and the exportin Cse1p cooperate to release Ulp1p from the karyopherins, indicating that stable sequestration of Ulp1p to the NPC would require a karyopherin-independent mechanism to anchor Ulp1p at the NPC.

Keywords: karyopherin; SUMO protease; Ulp1p; nuclear pore complex; nuclear localization signal

Abbreviations used: NLS, nuclear localization signal; SUMO, small ubiquitin-like

modifier; NPC, nuclear pore complex; PDB, protein data bank

Introduction

The small, ubiquitin-like modifiers (SUMOs) provide a reversible, post-translational modification mostly of nuclear proteins and regulate stability, localization, activity, or binding properties of target proteins that are involved in a wide range of cellular processes such as cell division, DNA repair, transcription, and mRNA quality control (reviewed in [1,2]). Like ubiquitin, SUMOs are synthesized as precursors that need to be processed to reveal the C-terminal di-glycine motifs before being conjugated to the target proteins. Conjugation of SUMO requires the action of a cascade of enzymes related to the ubiquitin E1, E2, and E3 ligases. Reversal of this modification is carried out by desumoylating enzymes (SUMO proteases) termed Ubl (ubiquitin-like protein)-specific proteases (Ulp) in yeast and sentrin-specific proteases (SENP) in vertebrates (reviewed in [3,4]).

In the budding yeast *Saccharomyces cerevisiae*, there are two SUMO proteases: the essential protein Ulp1p [5] and the nonessential protein Ulp2p (also known as Smt4p) [6,7]. Ulp1p is also responsible for SUMO precursor maturation [5]. Importantly, the substrate specificity of Ulp1p and Ulp2p is strongly influenced by their restricted subcellular localization. Ulp1p is localized primarily at the nuclear pore complex (NPC) and is concentrated at the nuclear periphery, whereas Ulp2p is found throughout the nucleoplasm [6,7]. Although the precise mechanism governing the NPC-localization of Ulp1p remains poorly understood, currently available data suggest that the sequestration of Ulp1p at the NPC depends on interactions involving the N-terminal noncatalytic domain of Ulp1p, karyopherins (Kap95p, Kap60p, and Kap121p), a subset of nucleoporins (the Nup84p complex and the Nup60p-Mlp1p-Mlp2p complex), and the nuclear envelope protein Esc1p [8,9,10,11,12].

The karyopherins (Kap95p, Kap60p, and Kap121p) that bind to Ulp1p are best known as nuclear import receptors (importins) essential for viability of yeast cells. Nuclear import of macromolecules is a signal-mediated active transport whose direction is determined by a gradient of the small GTPase Ran (Gsp1p in yeast), which cycles between GDP- and GTP-bound states and regulates karyopherin-cargo interactions (reviewed in [13]). The localization of Ran GTPase-activating protein (RanGAP) to the cytoplasm leads to Ran (Gsp1p) being predominantly in the GDP-bound state in the cytoplasm, whereas the nuclear localization of Ran guanine nucleotide exchange factor (RanGEF; RCC1) leads to Ran (Gsp1p) being predominantly in the GTP-bound state in the nucleus. In general, karyopherins bind cargo in the cytoplasm by recognizing the nuclear localization signal (NLS) of the cargo, and release cargo in the nucleus because Ran-GTP displaces the NLS from the karyopherins (reviewed in [13]).

The karyopherins Kap95p (yeast importin-β) and Kap60p (yeast importin-α) form a heterodimer that mediates nuclear import of numerous proteins containing the classical NLSs (cNLSs) that fall into two distinct classes termed monopartite cNLSs, containing a single cluster of basic amino acids, and bipartite cNLSs, containing two clusters of basic residues separated by a linker of variable length (reviewed in [14]). The structural basis for nuclear import mediated by Kap60p-Kap95p heterodimer has been well established (reviewed in [14]). Kap60p is composed of two domains: the N-terminal importin-β-binding (IBB) domain, and the C-terminal domain built from 10 tandem ARM repeats. The ARM repeat domain of Kap60p has an elongated shape and cNLSs bind along the groove on the concave surface of the ARM repeat domain. The IBB domain of Kap60p in turn binds to Kap95p, forming a ternary cargo-Kap60p-Kap95p complex in the cytoplasm. In the nucleus, Gsp1p-GTP binds to Kap95p and displaces the IBB domain of Kap60p from Kap95p. The dissociated IBB

domain has an autoinhibitory activity and binds to the cNLS-binding sites of Kap60p, releasing the cNLS-containing proteins. The cargo-free Kap60p forms a ternary complex with the exportin Cse1p (yeast Exportin-2) and Gsp1p-GTP, and is recycled back to the cytoplasm. The Kap95p-Gsp1p-GTP complex also exits the nucleus. In the cytoplasm, both Cse1p-Kap60p-Gsp1p-GTP complex and Kap95p-Gsp1p-GTP complex are disassembled due to the action of Rna1p (yeast RanGAP) and Yrb1p (yeast RanBP1). The dissociated Kap60p and Kap95p can then participate in another import cycle.

The karyopherin Kap121p (also known as Pse1p) is a member of karyopherin-β superfamily (reviewed in [15]) and mediates nuclear import of proteins that carry the Kap121p-specific NLS termed isoleucine-lysine (IK)-NLS, which has a consensus amino acid sequence of K-V/I-x-K-x_{1-2}-K/H/R, in which the underlined two residues are critical as specificity determinants and are minimally required for binding to Kap121p [16,17]. Kap121p has a superhelical structure constructed from 24 tandem HEAT repeats, and the binding site for the IK-NLS is located on the inner surface of HEAT repeats 7-12 [16,17]. In the nucleus, Gsp1p-GTP binds to Kap121p and displaces the IK-NLS-containing proteins. Like Kap95p, Kap121p-Gsp1p-GTP complex exits the nucleus. In the cytoplasm, the Kap121p-Gsp1p-GTP complex is disassembled, and free Kap121p participates in another import cycle.

Previous studies showed that the N-terminal noncatalytic domain of Ulp1p is necessary and sufficient for NPC targeting [8,9]. The N-terminal domain of Ulp1p contains the Kap121p-binding region (residues 1-150) and the Kap60p-Kap95p-binding region (residues 150-340), and it has been suggested that Ulp1p binds to the karyopherins Kap95p, Kap60p, and Kap121p through Gsp1p-GTP-insensitive unconventional interactions [9]. We report here, however, that our structural analyses of

Ulp1p-karyopherin interactions, combined with biochemical analyses, demonstrate that Ulp1p in fact has canonical NLSs and can be released from the karyopherins through concerted actions of Gsp1p-GTP and Cse1p.

Results

Ulp1p binds to the NLS-binding site of Kap121p and is dissociated from Kap121p by Gsp1p-GTP

As a first step toward elucidating the structural basis for Ulp1p-karyopherin interactions, we crystallized a complex formed between Kap121p (Δ80-90; a functional deletion mutant suitable for crystallization [16]) and the N-terminal region of Ulp1p (residues 1-150), which was identified as the Kap121p-binding region by Panse *et al*. in a previous study [9]. The crystals belonged to space group $P2_12_12_1$ and diffracted X-rays to 2.8 Å resolution (Table 1). The Kap121p-Ulp1p co-crystals were isomorphous to the previously obtained crystals of Kap121p-Ste12p complex, Kap121p-Pho4p complex, Kap121p-Nup53p complex, and Kap121p-Cdc14p complex [16,17]. Among these previously determined structures of Kap121p-ligand complexes, the structure of Kap121p-Ste12p complex was of the highest resolution, and so was used as a model to determine the structure of Kap121p-Ulp1p complex using molecular replacement. Electron density map based on the Kap121p model, following refinement, clearly showed extra electron density of a five-residue peptide, most likely Ulp1p residues 51-55 (^{51}GIYKK^{55}), bound to the NLS-binding site of Kap121p on the inner surface of HEAT repeats 8-12 (Fig. 1a). No reliable electron density corresponding to Ulp1p was observed elsewhere on Kap121p. After building the Ulp1p model, the structure was finally refined to free and working *R*-factor values of 24.1% and 19.8%, respectively (Table 1).

The overall structure of Kap121p in the Kap121p-Ulp1p complex was quite similar to that of Kap121p-NLS complexes reported previously [16,17]. Ulp1p adopted an extended conformation and occupied the critical P1 and P2 pockets at the

NLS-binding site: the hydrophobic side chain of $I52^{Ulp1p}$ fitted into the nonpolar P1 pocket formed by C429, N430, G433, Q434, H470, and A474 of Kap121p; the side chain of $K54^{Ulp1p}$ bound to the acidic P2 pocket through salt bridges with $D353^{Kap121p}$ and $E396^{Kap121p}$. The position and orientation of Ulp1p on Kap121p was further stabilized by hydrogen bonds formed between the main chain atoms of $I52^{Ulp1p}$ and the side chain of $N477^{Kap121p}$ (Fig. 1b,c). In contrast to the side chains of $I52^{Ulp1p}$ and $K54^{Ulp1p}$ that had well-ordered electron density, the side chains of $Y53^{Ulp1p}$ and $K55^{Ulp1p}$ did not have well-defined density, and so were probably disordered. Thus, two residues of Ulp1p, an isoleucine and a lysine, appeared to be critical for the specific binding to Kap121p, as was the case in the structure of Kap121p-Cdc14p complex [17].

Although the atomic model depicted in Figure 1b appeared to be the most plausible interpretation of the density map, inspection of the Ulp1p amino acid sequence indicated that Ulp1p residues 4-8 (^{4}E<u>V</u>D<u>K</u>H^{8}) fulfill the minimal requirement as an IK-NLS and might also be able to bind to the NLS-binding site of Kap121p, with the underlined valine and lysine residues binding to the P1 and P2 pockets, respectively. We examined this possibility using engineered mutants of Ulp1p and GST pull-down assay. As shown in Figure 2a, the double mutations V5A/K7A of Ulp1p did not affect the binding to Kap121p appreciably, whereas the single mutation K54A of Ulp1p drastically decreased the binding to Kap121p to an undetectable level. Thus, mutational analyses verified our interpretation of the electron density map.

The observation that Ulp1p binds only to the NLS-binding site of Kap121p just like canonical nuclear import cargoes immediately suggested that the binding of Ulp1p to Kap121p is in fact sensitive to Gsp1p-GTP. This idea was indeed supported by GST pull-down assay. As shown in Figure 2b, Gsp1p-GDP did not compete with Ulp1p to bind Kap121p but Gsp1p-GTP inhibited the binding of Ulp1p to Kap121p. Thus,

although our initial purpose of this study was to find a novel mechanism of Gsp1p-insensitive ligand recognition by Kap121p, the structure of Kap121p-Ulp1p complex and biochemical analyses unexpectedly showed that Ulp1p has a canonical IK-NLS that can be dissociated from Kap121p by Gsp1p-GTP.

Ulp1p binds to the major- and minor- classical NLS binding sites of Kap60p

To further characterize Ulp1p-karyopherin interactions, we next determined the crystal structure at 2.5 Å resolution of a complex formed between the NLS-binding ARM repeat domain of Kap60p (residues 88-510) and residues 150-340 of Ulp1p, which constitute the Kap60p-Kap95p-binding region [9] (Table 1). The crystals belonged to space group *P*1 and had two complexes in the asymmetric unit. The structure was determined using molecular replacement and refined to free and working *R*-factor values of 24.7% and 21.4%, respectively (Table 1). Electron density corresponding to Ulp1p residues 154-172 was unambiguously identified on the concave surface of Kap60p in both complexes in the asymmetric unit, whereas residues 150-153 and 173-340 of Ulp1p had no interpretable electron density. We therefore crystallized a complex formed between Ulp1p residues 150-172 and the ARM repeat domain of Kap60p, and obtained better-ordered crystals that diffracted X-rays to 2.2 Å resolution and belonged to space group $P2_12_12_1$ (one complex in the asymmetric unit) (Table 1). The crystal structure of the $P2_12_12_1$ form was refined to free and working *R*-factor values of 22.8% and 20.2%, respectively (Table 1). The following description of the structure of Kap60p-Ulp1p complex is based on the higher resolution structure of the $P2_12_12_1$ form, which was essentially identical to the structure of the *P*1 form (Fig. S1).

The Ulp1p residues 154-172 (^{154}RKHKFDTSTWALPNKRRRI^{172}) bound along the surface groove of Kap60p in an almost fully extended conformation (Fig. 3),

as observed in a number of previously determined co-crystal structures of importin-α/Kap60p bound to bipartite classical NLSs (reviewed in [14,18,19]). As illustrated in detail in Figure 4a, 4b, and 4c, Ulp1p made extensive main chain and side chain interactions with Kap60p at the minor- and major- NLS binding sites located in ARM repeats 6-8 and 2-4, respectively.

At the minor NLS-binding site (Fig. 4a), $K155^{Ulp1p}$ in the P1' position made hydrogen bonds with the side chain of $T334^{Kap60p}$ and the main-chain carbonyls of $V327^{Kap60p}$ and $N367^{Kap60p}$; the imidazole ring of $H156^{Ulp1p}$ in the P2' position was sandwiched between the indole rings of $W405^{Kap60p}$ and $W363^{Kap60p}$, and made a hydrogen bond with $E402^{Kap60p}$; $K157^{Ulp1p}$ in the P3' position formed a hydrogen bond with $N325^{Kap60p}$; $F158^{Ulp1p}$ in the P4' position packed against the indole ring of $W363^{Kap60p}$. In addition, the main chain of $H156^{Ulp1p}$ formed hydrogen bonds with $N367^{Kap60p}$ and $W363^{Kap60p}$.

At the major NLS-binding site (Fig. 4b), $N167^{Ulp1p}$ in the P1 position formed a hydrogen bond with $W237^{Kap60p}$; $K168^{Ulp1p}$ in the P2 position formed a salt bridge with $D203^{Kap60p}$, and also formed hydrogen bonds with $T166^{Kap60p}$ and a main-chain carbonyl of $G161^{Kap60p}$; $R169^{Ulp1p}$ in the P3 position formed a salt bridge with $D276^{Kap60p}$ and hydrophobic/cation-π interactions with $W237^{Kap60p}$; $R170^{Ulp1p}$ in the P4 position formed hydrogen bonds with $S160^{Kap60p}$ and a main-chain carbonyl of $E118^{Kap60p}$; the aliphatic portion of the side chain of $R171^{Ulp1p}$ in the P4 position was sandwiched between the indole rings of $W195^{Kap60p}$ and $W153^{Kap60p}$. These interactions were supplemented with hydrogen bonds between the main chain of Ulp1p and $R244^{Kap60p}$, $G202^{Kap60p}$, $N241^{Kap60p}$, $N199^{Kap60p}$, $N157^{Kap60p}$, and $W153^{Kap60p}$.

The linker residues (^{159}DTSTWALP^{166}) connecting the two clusters of the

basic residues of Ulp1p did not make direct contacts with Kap60p, except for the hydrophobic side chains of W163, L165, and P166, which contacted nonpolar indentations on the outer surface of ARM repeat 10 of an adjacent Kap60p molecule in the crystal. It may be that these crystal packing interactions influenced the conformation of the linker residues of Ulp1p.

We used mutants of Ulp1p to evaluate the contributions made by the basic residues of Ulp1p for the binding to Kap60p in solution (Fig. 4d). In GST pull-down assays, substitution of K155 with alanine reduced the binding of Ulp1p (residues 150-172) to ΔIBB Kap60p slightly (Fig. 4d, lane 3), whereas substitution of K168 with alanine reduced the binding to an undetectable level (Fig. 4d, lane 4). The binding of the double mutant K155A/K168A of Ulp1p (residues 150-172) was also undetectably weak (Fig. 4d, lane 5). These results suggest that not all basic residues of Ulp1p are equally important for Kap60p-binding and that the basic residue (K168) that occupies the P2 position in the major site makes a key contribution in Kap60p-binding.

Gsp1p-GTP (Ran-GTP) and Cse1p (Exportin-2) cooperate to disassemble the Ulp1p-Kap60p-Kap95p (SENP2-importin-α:β) complex

Our structural data that Ulp1p binds to the cNLS-binding sites of Kap60p raised a possibility that the binding of Ulp1p to the karyopherins Kap60p and Kap95p is in fact sensitive to Gsp1p-GTP, just like ordinary cNLS-containing nuclear import cargoes. We used GST pull-down assays to test this possibility (Fig. 5a). The full-length Kap60p and Kap95p bound to GST-Ulp1p (residues 150-172) (Fig. 5a, lane 2) but not to GST alone (Fig. 5a, lane 1), confirming the specific binding of Kap60p-Kap95p heterodimer to Ulp1p residues 150-172. In the presence of Gsp1p-GTP (Fig. 5a, lane 4), but not Gsp1p-GDP (Fig. 5a, lane 3), the binding of Kap95p was weakened

dramatically but Kap60p still remained bound to Ulp1p residues 150-172. However, when the assay was done in the presence of both Cse1p and Gsp1p-GTP (but not Gsp1p-GDP), both Kap95p and Kap60p were released from Ulp1p residues 150-172 (Fig. 5a, lanes 5 and 6). These results suggest that Gsp1p-GTP can displace Kap95p from Kap60p and, although the binding of Ulp1p to Kap60p is so strong that the autoinhibitory activity of the IBB domain of Kap60p is not sufficient to displace Ulp1p from Kap60p, the combined actions of Cse1p and Gsp1p-GTP can displace Kap60p from Ulp1p.

The strong binding of Ulp1p residues 150-172 to the full-length Kap60p containing the autoinhibitory IBB domain was reminiscent of the observation previously reported by Goeres *et al*. [20] that SENP2, one of the mammalian SUMO proteases, has a bipartite NLS in the N-terminal region (residues 1-63) that binds to full-length importin-α with high affinity. Although Goeres *et al*. inferred that the unusually stable association of SENP2 with importin-α may prevent dissociation upon entry into the nucleus [20], we hypothesized that Exportin-2 (mammalian homologue of yeast Cse1p) may be able to work together with Ran-GTP to displace importin-α from SENP2, because Exportin-2 (Cse1p) and Ran-GTP (Gsp1p-GTP) can strengthen the autoinhibitory activity of the IBB domain to displace cNLSs from importin-α (Kap60p) [21]. We used GST pull-down assay to test this hypothesis. To prevent proteolysis of SENP2, we co-expressed GST-SENP2 (residues 1-63) and importin-α in bacteria, and immobilized the purified complex on Glutathione-sepharose beads. The binding of importin-β (Kapβ1) to this complex was readily detectable (Fig. 5b, lane 6). Ran-GTP, but not Ran-GDP, promoted dissociation of importin-β (Fig. 5b, lanes 7 and 8), but importin-α still remained bound to SENP2 (residues 1-63) even in the presence of Ran-GTP (Fig. 5b, lanes 7 and 8). However, when both Exportin-2 and Ran-GTP (but not Ran-GDP) were added together, both importin-α and importin-β dissociated from

SENP2 (residues 1-63) (Fig. 5b, lanes 9-10). These results support our idea that the N-terminal NLS of SENP2 can be displaced from importin-α and importin-β through concerted action of Exportin-2 and Ran-GTP.

We also performed binding assays using GST-Ulp1p (residues 150-340) instead of GST-Ulp1p (residues 150-172) (Fig. 5c). Remarkably, Kap95p remained bound to Kap60p and Ulp1p (residues 150-340) even in the presence of Gsp1p-GTP (Fig. 5c, lane 4), and both Cse1p and Gsp1p-GTP were required to cause dissociation of Kap95p (Fig. 5c, lane 6), suggesting that Ulp1p residues 150-340 contain direct binding site for Kap95p in addition to the classical bipartite NLS sequence (residues 154-172) that bind to Kap60p. Indeed, GST pull-down assay showed that Kap95p directly bind to Ulp1p residues 150-340 (Fig. 5d, lane 2). This direct interaction between Kap95p and Ulp1p was dramatically weakened by Gsp1p-GTP (Fig. 5d, lane 4) but only slightly weakened by Gsp1p-GDP (Fig. 5d, lane 3). To probe how Ulp1p binds to Kap95p, we examined whether the IBB domain of Kap60p competes with Ulp1p for the binding to Kap95p (Fig. 5e). Interestingly, IBB-GFP did not compete with Ulp1p for the binding to Kap95p and, instead, strengthened the binding of Kap95p to Ulp1p (residues 150-340), forming a ternary complex with Kap95p and Ulp1p (Fig. 5e, lane 2). GFP did not affect the binding of Kap95p to Ulp1p (Fig. 5e, lane 3), and both IBB-GFP and GFP did not bind to Ulp1p (residues 150-340) (Fig. 5e, lanes 4 and 5), and so the data in lane 2 of Figure 5e suggest that IBB indirectly binds to Ulp1p via Kap95p. Unfortunately we have been unable to crystallize Kap95p in complex with Ulp1p (both in the presence and absence of the IBB domain of Kap60p), and so the structural basis for the Kap95p-Ulp1p interactions remains unclear. Nevertheless, our biochemical data demonstrate that the assembly of the Ulp1p-Kap60p-Kap95p complex is highly cooperative and that the disassembly of the ternary complex requires concerted action of both Gsp1p-GTP and Cse1p.

Discussion

In this study, we have characterized the interactions between the N-terminal non-catalytic domain of Ulp1p and the karyopherins (Kap60p, Kap95p, and Kap121p) using X-ray crystallography and solution binding assays. It was previously suggested that the N-terminal domain of Ulp1p binds the karyopherins in a Gsp1p-GTP-insensitive manner [9], and so we initially expected to find novel mechanism of the interactions between the karyopherins and their binding partner. Unexpectedly, however, our structural and biochemical data have identified a canonical IK-NLS and a bipartite cNLS in the N-terminal non-catalytic domain of Ulp1p. The Kap121p-specific IK-NLS (Ulp1p residues 51-55) binds to the NLS-binding site located on the HEAT repeats 8-12 of Kap121p, and is dissociated by Gsp1p-GTP, just like well-characterized nuclear import cargo such as Pho4p and Ste12p. Although it is unclear why our results (regarding the sensitiveness of the Ulp1p-Kap121p interaction to Gsp1p-GTP) disagree with the observations previously reported by Panse *et al*. [9], our structural data are totally consistent with our biochemical data. The cNLS of Ulp1p (residues 154-172) binds along the major- and minor-NLS binding sites of the ARM repeat domain of Kap60p and, although it has high affinity to Kap60p, it can be dissociated from Kap60p by the concerted action of Cse1p and Gsp1p-GTP, probably because Cse1p and Gsp1p-GTP strengthen the autoinhibitory activity of the IBB domain [21]. Our binding studies have also shown that Ulp1p binds Kap95p directly, and that Ulp1p can be efficiently released from Kap95p by Gsp1p-GTP. The interaction between Ulp1p and Kap95p is also weakened, albeit only slightly, by Gsp1p-GDP, possibly because Kap95p can bind weakly (with micromolar affinity) to Gsp1p-GDP by inducing conformational changes in the switch loops of Gsp1p to adopt the GTP-bound conformation [22]. A notable feature of the Ulp1p-Kap95p binding is that the binding is enhanced by the IBB domain of Kap60p. Thus, Ulp1p, Kap60p, and Kap95p assemble

cooperatively into a stable ternary complex that is resistant to disassembly by Gsp1p-GTP. However, our binding data have shown that, although Gsp1p-GTP alone is unable to disassemble the ternary Ulp1p-Kap60p-Kap95p complex as proposed previously [9], the ternary complex can be efficiently disassembled in the presence of both Gsp1p-GTP and Cse1p.

Because the Kap121p-binding site (Ulp1p residues 51-55) and the binding sites for Kap60p-Kap95p (Ulp1p residues 150-340) are distinct, Ulp1p would be able to bind Kap121p and Kap60p-Kap95p simultaneously. The association of Ulp1p with as many as three karyopherins (Kap121p, Kap60p, and Kap95p) could stabilize the binding of Ulp1p to the NPC through the karyopherins. Thus, Kap121p, Kap60p, and Kap95p would promote docking of Ulp1p to the NPC. However, it seems quite unlikely that the karyopherin-mediated docking of Ulp1p to the NPC is permanent, because Gsp1p-GTP and Cse1p would efficiently promote dissociation of karyopherins from Ulp1p on the nuclear face of the NPC. In the light of our structural and biochemical data, it seems most likely that the karyopherins Kap121p, Kap60p, and Kap95p mediate nuclear import of Ulp1p and, after NPC passage, Ulp1p is released from the karyopherins by the concerted action of Gsp1p-GTP and Cse1p in the nucleus. Thus our findings disagree with the so-far prevailing notion that Ulp1p is tethered to the transport channel of the NPC through unconventional interactions with the karyopherins [9], and indicate that stable sequestration of Ulp1p to the NPC would require a karyopherin-independent mechanism to anchor Ulp1p at the NPC. One possibility would be that, after entry into the nucleus and dissociation of the karyopherins, Ulp1p binds to the nucleoplasmic face of the NPC through direct binding to nucleoporins or through adapter proteins (besides karyopherins) that bind both nucleoporins and Ulp1p. The comprehensive identification of binding partners of Ulp1p at the NPC remains a challenge and would require extensive analysis of the interactions between Ulp1p and

the NPC.

Materials and Methods

Protein expression and purification

To prepare Kap121p-Ulp1p complex for crystallization, GST-Kap121p (Δ80-90) [16] and His-Ulp1p (*S. cerevisiae*, residues 1-150; TEV cleavage site was inserted between the His-tag and Ulp1p) were co-expressed from pGEX-TEV [21] and pRSFDuet-1 (Novagen), respectively, in the *E. coli* host strain BL21-CodonPlus(DE3)RIL (Stratagene). The cells were harvested, resuspended in buffer A [30 mM Tris-HCl (pH 7.5), 150 mM NaCl, 10 mM imidazole, 7 mM 2-mercaptoethanol, 0.5 mM phenylmethylsulfonyl fluoride (PMSF), and 0.5 mM 4-(2-aminoethyl) benzenesulfonyl fluoride hydrochloride (AEBSF)], and lysed by sonication on ice. All subsequent purification steps were performed at 4 °C. Clarified lysates were loaded onto Ni-NTA resin (Novagen), washed with buffer A containing 25 mM imidazole, and eluted with buffer A containing 250 mM imidazole. Tween-20 was added to the eluate to a final concentration of 0.05%. After incubating the Ni-NTA eluate with glutathione-Sepharose 4B resin (GE Healthcare), the resin was washed with buffer B [10 mM Tris-HCl (pH 7.5), 120 mM NaCl, 0.05% Tween-20, and 2 mM 2-mercaptoethanol]. The GST- and His-tags were cleaved off Kap121p and Ulp1p by incubating the resin overnight with His-TEV protease (0.1 mg/ml) in buffer B containing 0.2 mM AEBSF. The Kap121p-Ulp1p complex, released from the resin, was finally purified by gel filtration over Superdex200 (GE Healthcare) in buffer B without Tween-20 and the complex was concentrated to 30 mg/ml using a 3 kDa molecular weight cutoff Amicon Ultra centrifugal filter (Millipore).

To prepare Kap60p-Ulp1p complex for crystallization, GST-Ulp1p (*S. cerevisiae*, residues 150-340 or residues 150-172) and untagged Kap60p (*S. cerevisiae*,

residues 88-510) were co-expressed from pGEX-TEV and pRSFDuet-1 (Novagen), respectively, in the *E. coli* host strain BL21-CodonPlus(DE3)RIL (Stratagene). The cells were harvested, resuspended in buffer C [10 mM Tris-HCl (pH 7.5), 150 mM NaCl, 1 mM EDTA, 7 mM 2-mercaptoethanol, 1 mM PMSF, and 0.2 mM AEBSF], and lysed by sonication on ice. All subsequent purification steps were performed at 4 °C. Tween-20 was added to 0.05%, and the clarified lysate was incubated with glutathione-Sepharose 4B resin (GE Healthcare) for 4 h. After washing the resin with buffer D [10 mM Tris-HCl (pH 7.5), 150 mM NaCl, 0.05% Tween-20, and 2 mM 2-mercaptoethanol], the GST-tag was cleaved off Ulp1p by incubating the resin overnight with His-TEV protease (0.02 mg/ml) in buffer D containing 0.2 mM AEBSF. The Kap60p-Ulp1p complex, released from the resin, was finally purified by gel filtration over Superdex200 (GE Healthcare) in buffer D without Tween-20 and the complex was concentrated to 15 mg/ml using a 3 kDa molecular weight cutoff Amicon Ultra centrifugal filter (Millipore).

The recombinant proteins for GST pull-down assays were expressed in the *E. coli* host strain BL21-CodonPlus(DE3)RIL (Stratagene). GST-Ulp1p (*S. cerevisiae*, residues 1-150 or residues 150-172 or residues 150-340) was expressed from pGEX-TEV, and purified over glutathione-Sepharose 4B (GE Healthcare) and gel filtration over Superdex200 (GE Healthcare). GST-Kap121p (*S. cerevisiae*, full-length) [16] was expressed from pGEX-TEV and initially purified over glutathione-Sepharose 4B (GE Healthcare). After removal of the GST tag by His-TEV protease, Kap121p was finally purified by gel filtration over Superdex200. GST-Cse1p (*S. cerevisiae*, full-length) [21] and GST-Exportin-2 (human, full-length) were expressed from pGEX-TEV and initially purified over glutathione-Sepharose 4B (GE Healthcare). After removal of the GST tag by His-TEV protease, Cse1p and Exportin-2 were finally purified by gel filtration over Superdex200. GST-SENP2 (human, residues 1-63) and

un-tagged importin-α1 (mouse, full-length) were co-expressed from pGEX-TEV and pRSFDuet-1 (Novagen), respectively. The complex formed between GST-SENP2 (residues 1-63) and importin-α1 was purified over glutathione-Sepharose 4B (GE Healthcare) and gel filtration over Superdex200 (GE Healthcare). His/S-importin-β1 (Kapβ1, mouse, full-length) [23] and His/S-Kap95p (*S. cerevisiae*, full-length) were expressed from pET30a-TEV [21]. His/S-Ran (canine, full-length), His/S-Kap60p (*S. cerevisiae*, full-length) and His/S-ΔIBB Kap60p (*S. cerevisiae*, residues 88-542) were expressed from pET30a [21,24]. His-Gsp1p (*S. cerevisiae*, full-length) was expressed from pET15b [24]. His-GFP-His and His-IBB (Kap60p residues 2-63)-GFP-His were expressed from pET28a (Novagen). The His-tagged proteins were purified over Ni-NTA (Novagen) and by gel filtration over Superdex200 or Superdex75 (GE Healthcare). Mutants were created using the QuickChange system (Stratagene). All DNA constructs were verified by DNA sequencing.

Crystallization and data collection

Crystals of Kap121p (Δ80-90)-Ulp1p (1-150) complex were grown by the hanging drop vapor diffusion technique. The protein (30 mg/ml in the final gel filtration buffer) was mixed 1:1 with reservoir solution containing 0.1 M HEPES (pH 7.0), 10% 2-propanol, and 24% PEG20000. The crystallization setups were left to equilibrate at 20 °C. Crystals were cryoprotected using reservoir solution containing 10% glycerol (but without 2-propanol) and flash-cooled in liquid nitrogen. An X-ray diffraction dataset was collected up to 2.8 Å resolution at 100 K at SPring-8 beamline BL41XU. The crystals belonged to the $P2_12_12_1$ space group (unit cell dimensions: a = 76.83 Å, b = 124.71 Å, c = 130.00 Å, $\alpha = \beta = \gamma = 90^\circ$) with one complex in the asymmetric unit.

Crystals of Kap60p (88-510)-Ulp1p (150-340) complex were grown by the

hanging drop vapor diffusion technique. The protein (8 mg/ml protein in the final gel filtration buffer) was mixed 1:1 with reservoir solution containing 0.1 M MES (pH 5.5), 0.1 M calcium acetate, 12% PEG8000. The crystallization setups were left to equilibrate at 20 °C. Crystals were cryoprotected using reservoir solution containing 20% PEG8000 and 23% glycerol and flash-cooled in liquid nitrogen. An X-ray diffraction dataset was collected up to 2.5 Å resolution at 100 K at Photon Factory beamline BL-1A. The crystals belonged to the *P*1 space group (unit cell dimensions: a = 53.61 Å, b = 63.54 Å, c = 80.91 Å, α = 106.09º, β = 107.72º, γ = 90.50º) with two complexes in the asymmetric unit.

Crystals of Kap60p (88-510)-Ulp1p (150-172) complex were grown by the hanging drop vapor diffusion technique. The protein (5 mg/ml in the final gel filtration buffer) was mixed 1:1 with reservoir solution containing 0.1 M sodium phosphate (pH 6.5), 12% PEG8000. The crystallization setups were left to equilibrate at 20 °C. Crystals were cryoprotected using reservoir solution containing 20% PEG8000 and 23% glycerol and flash-cooled in liquid nitrogen. An X-ray diffraction dataset was collected up to 2.2 Å resolution at 100 K at Photon Factory beamline BL-17A. The crystals belonged to the $P2_12_12_1$ space group (unit cell dimensions: a = 53.82 Å, b = 64.25 Å, c = 91.40 Å, $\alpha = \beta = \gamma = 90$º) with one complex in the asymmetric unit.

Structure determination and refinement

Diffraction data were processed using MOSFLM and CCP4 programs [25]. The structure of Kap121p (Δ80-90)-Ulp1p (1-150) complex was solved by molecular replacement using MOLREP [26] using the structure of Kap121p-Ste12p complex (PDB code, 3W3W) [16] as a search model. The structure was refined by iterative cycles of model building using COOT [27] and refinement using REFMAC5 [28] and

PHENIX [29]. TLSMD analyses [30] were used to define TLS groups for the final cycles of refinement. The final model contained Kap121p residues 3-79, 91-545, 550-590, 596-658, 663-735, 740-811, 817-821, 828-951, 954-978, 986-1017, 1021-1045, 1049-1064, 1068-1088, and Ulp1p residues 51-55. MolProbity [31] was used to validate the final model.

The structure of Kap60p (88-510)-Ulp1p (150-340) complex was solved by molecular replacement using MOLREP [26] using the structure of Kap60p-Nup2p complex (PDB code, 2C1T) [32] as a search model. The structure was refined by iterative cycles of model building using COOT [27] and refinement using REFMAC5 [28] and PHENIX [29]. The final model contained two molecules of Kap60p residues 88-465, 471-510, two molecules of Ulp1p residues 154-172, and 85 water molecules. MolProbity [31] was used to validate the final model.

The structure of Kap60p (88-510)-Ulp1p (150-172) was solved by molecular replacement using MOLREP [26] using the structure of Kap60p (88-510)-Ulp1p (150-340) complex as a search model. The structure was refined by iterative cycles of model building using COOT [27] and refinement using PHENIX [29]. The final model contained Kap60p residues 88-465, 471-510, Ulp1p residues 154-172, and 220 water molecules. MolProbity [31] was used to validate the final model.

Structural figures were produced using CCP4MG [33], Molscript [34], and Raster3D [35].

GST pull-down assay

Pull-down assays were performed in binding buffer (phosphate-buffered

saline, 0.1% Tween-20, 0.2 mM DTT, and 0.2 mM PMSF). GST-fusion proteins were immobilized on 10 μl of packed glutathione-Sepharose 4B (GE Healthcare) beads and each binding reaction was performed by incubating the beads with reaction mixtures in a total volume of 50 μl for 1 h at 4 °C. The amounts of proteins used are indicated in the figure legends. Beads were then spun down and washed twice with 1 ml of binding buffer, and bound proteins were analyzed by SDS-PAGE (sodium dodecyl sulfate-polyacrylamide gel electrophoresis) and Coomassie staining.

Protein Data Bank accession codes

Atomic coordinates and structure factors have been deposited in the Protein Data Bank with accession codes 5H2V [Kap121p (Δ80-90)-Ulp1p (1-150) complex], 5H2W [Kap60p (88-510)-Ulp1p (150-340) complex], and 5H2X [Kap60p (88-510)-Ulp1p (150-172) complex].

Acknowledgements

We thank Masako Koyama and Ryohei Nakada for assistance and discussion. We are indebted to the staff of SPring-8 and Photon Factory for assistance during data collection. The X-ray diffraction data collection experiments at the beamline BL41XU of SPring-8 were performed with the approval of the Japan Synchrotron Radiation Research Institute (Proposal No. 2011B1083). This work was supported by JSPS/MEXT KAKENHI (25440019) and the Kurata Memorial Hitachi Science and Technology Foundation.

References

[1] Melchior F. SUMO--nonclassical ubiquitin. Annu Rev Cell Dev Biol. 2000;16:591-626.

[2] Johnson ES. Protein modification by SUMO. Annu Rev Biochem. 2004;73:355-82.

[3] Mukhopadhyay D, Dasso M. Modification in reverse: the SUMO proteases. Trends Biochem Sci. 2007;32:286-95.

[4] Hickey CM, Wilson NR, Hochstrasser M. Function and regulation of SUMO proteases. Nat Rev Mol Cell Biol. 2012;13:755-66.

[5] Li SJ, Hochstrasser M. A new protease required for cell-cycle progression in yeast. Nature. 1999;398:246-51.

[6] Li SJ, Hochstrasser M. The yeast ULP2 (SMT4) gene encodes a novel protease specific for the ubiquitin-like Smt3 protein. Mol Cell Biol. 2000;20:2367-77.

[7] Schwienhorst I, Johnson ES, Dohmen RJ. SUMO conjugation and deconjugation. Mol Gen Genet. 2000;263:771-86.

[8] Li SJ, Hochstrasser M. The Ulp1 SUMO isopeptidase: distinct domains required for viability, nuclear envelope localization, and substrate specificity. J Cell Biol. 2003;160:1069-81.

[9] Panse VG, Kuster B, Gerstberger T, Hurt E. Unconventional tethering of Ulp1 to the transport channel of the nuclear pore complex by karyopherins. Nat Cell Biol. 2003;5:21-7.

[10] Zhao X, Wu CY, Blobel G. Mlp-dependent anchorage and stabilization of a desumoylating enzyme is required to prevent clonal lethality. J Cell Biol. 2004;167:605-11.

[11] Palancade B, Liu X, Garcia-Rubio M, Aguilera A, Zhao X, Doye V. Nucleoporins prevent DNA damage accumulation by modulating Ulp1-dependent sumoylation processes. Mol Biol Cell. 2007;18:2912-23.

[12] Lewis A, Felberbaum R, Hochstrasser M. A nuclear envelope protein linking nuclear pore basket assembly, SUMO protease regulation, and mRNA surveillance. J Cell Biol. 2007;178:813-27.

[13] Gorlich D, Kutay U. Transport between the cell nucleus and the cytoplasm. Annu Rev Cell Dev Biol. 1999;15:607-60.

[14] Stewart M. Molecular mechanism of the nuclear protein import cycle. Nat Rev Mol Cell Biol. 2007;8:195-208.

[15] Chook YM, Suel KE. Nuclear import by karyopherin-betas: Recognition and inhibition. Biochim Biophys Acta. 2010;1813:1593-606.

[16] Kobayashi J, Matsuura Y. Structural Basis for Cell-Cycle-Dependent Nuclear Import Mediated by the Karyopherin Kap121p. J Mol Biol. 2013;425:1852-68.

[17] Kobayashi J, Hirano H, Matsuura Y. Crystal structure of the karyopherin Kap121p bound to the extreme C-terminus of the protein phosphatase Cdc14p. Biochem Biophys Res Commun. 2015;463:309-14.

[18] Marfori M, Mynott A, Ellis JJ, Mehdi AM, Saunders NF, Curmi PM, et al. Molecular basis for specificity of nuclear import and prediction of nuclear localization. Biochim Biophys Acta. 2010;1813:1562-77.

[19] Christie M, Chang CW, Rona G, Smith KM, Stewart AG, Takeda AA, et al. Structural Biology and Regulation of Protein Import into the Nucleus. J Mol Biol. 2016;428:2060-90.

[20] Goeres J, Chan PK, Mukhopadhyay D, Zhang H, Raught B, Matunis MJ. The SUMO-specific isopeptidase SENP2 associates dynamically with nuclear pore complexes through interactions with karyopherins and the Nup107-160 nucleoporin subcomplex. Mol Biol Cell. 2011;22:4868-82.

[21] Matsuura Y, Stewart M. Structural basis for the assembly of a nuclear export complex. Nature. 2004;432:872-7.

[22] Forwood JK, Lonhienne TG, Marfori M, Robin G, Meng W, Guncar G, et al. Kap95p binding induces the switch loops of RanGDP to adopt the GTP-bound conformation: implications for nuclear import complex assembly dynamics. J Mol Biol. 2008;383:772-82.

[23] Hirano H, Matsuura Y. Sensing actin dynamics: structural basis for G-actin-sensitive nuclear import of MAL. Biochem Biophys Res Commun. 2011;414:373-8.

[24] Matsuura Y, Lange A, Harreman MT, Corbett AH, Stewart M. Structural basis for Nup2p function in cargo release and karyopherin recycling in nuclear import. EMBO J. 2003;22:5358-69.

[25] Winn MD, Ballard CC, Cowtan KD, Dodson EJ, Emsley P, Evans PR, et al. Overview of the CCP4 suite and current developments. Acta Crystallogr D Biol Crystallogr. 2011;67:235-42.

[26] Vagin A, Teplyakov A. Molecular replacement with MOLREP. Acta Crystallogr D Biol Crystallogr. 2010;66:22-5.

[27] Emsley P, Cowtan K. Coot: model-building tools for molecular graphics. Acta Crystallogr D Biol Crystallogr. 2004;60:2126-32.

[28] Murshudov GN, Skubak P, Lebedev AA, Pannu NS, Steiner RA, Nicholls RA, et al. REFMAC5 for the refinement of macromolecular crystal structures. Acta Crystallogr D Biol Crystallogr. 2011;67:355-67.

[29] Adams PD, Afonine PV, Bunkoczi G, Chen VB, Davis IW, Echols N, et al. PHENIX: a comprehensive Python-based system for macromolecular structure solution. Acta Crystallogr D Biol Crystallogr. 2010;66:213-21.

[30] Painter J, Merritt EA. Optimal description of a protein structure in terms of multiple groups undergoing TLS motion. Acta Crystallogr D Biol Crystallogr. 2006;62:439-50.

[31] Chen VB, Arendall WB, 3rd, Headd JJ, Keedy DA, Immormino RM, Kapral GJ, et al. MolProbity: all-atom structure validation for macromolecular crystallography. Acta Crystallogr D Biol Crystallogr. 2010;66:12-21.

[32] Matsuura Y, Stewart M. Nup50/Npap60 function in nuclear protein import complex disassembly and importin recycling. EMBO J. 2005;24:3681-9.

[33] McNicholas S, Potterton E, Wilson KS, Noble ME. Presenting your structures: the CCP4mg molecular-graphics software. Acta Crystallogr D Biol Crystallogr. 2011;67:386-94.

[34] Kraulis PJ. MOLSCRIPT: a program to produce both detailed and schematic plots of protein structures. Journal of applied crystallography. 1991;24:946-50.

[35] Merritt EA, Bacon DJ. Raster3D: photorealistic molecular graphics. Methods Enzymol. 1997;277:505-24.

Figure legends

Fig. 1. Crystal structure of Kap121p-Ulp1p complex (PDB code, 5H2V). (a) Ribbon representation of the overall structure of Kap121p (green) bound to Ulp1p (stick representation with orange carbons). The composite omit map (blue mesh, contoured at 1σ) covering Ulp1p is superposed. (b) Close-up view of the interactions involving Ulp1p IK-NLS (ball-and-stick representation with magenta carbons) with key residues of Kap121p (light gray) at the NLS-binding site. The B-helices of Kap121p HEAT repeats 8-11 are labeled 8B-11B. Dashed lines indicate hydrogen bonds or salt bridges. (c) The Ulp1p side chains of I52 and K54 fit into the pockets P1 and P2, respectively, at the NLS-binding site of Kap121p (surface representation colored by electrostatic potential: blue, positive; red, negative; white, neutral). The main chain of Ulp1p is shown in worm representation (green), with the side chains of I52 and K54 shown in ball-and-stick representation.

Fig. 2. GST pull-down assay verified the crystal structure of Kap121p-Ulp1p complex and provided evidence that Kap121p binds to Ulp1p in a Gsp1p-GTP-sensitive manner. (a) Immobilized 6 μg GST (lane 1) or 20 μg GST-Ulp1p (residues 1-150; lane 2, wild-type; lane 3, V5A/K7A mutant; lane 4, K54A mutant) was incubated with 20 μg Kap121p. (b) Immobilized 20 μg GST-Ulp1p (residues 1-150) was incubated with 2.7 μg Kap121p alone (lane 1) or 2.7 μg Kap121p together with 10 μg Gsp1p (lane 2, Gsp1p-GDP; lane 3, Gsp1p-GTP).

Fig. 3. Crystal structure of Kap60p-Ulp1p complex (PDB code, 5H2X). Two orthogonal views of the overall structure of Kap60p (ribbon representation in green) bound to the bipartite classical NLS of Ulp1p (stick representation with orange carbons) are shown. The composite omit map (blue mesh, contoured at 1σ) covering Ulp1p is superposed.

Fig. 4. Structural basis for the recognition of Ulp1p NLS by Kap60p. (a, b) Close-up views of the interactions between Kap60p (light gray) and Ulp1p (ball-and-stick representation with magenta carbons) at (a) the minor NLS-binding site and (b) the major NLS-binding site. (c) Schematic illustration of the interactions of Kap60p with Ulp1p. Dashed lines represent hydrogen bonds or salt bridges. The minor-site positions P1'-P4' and the major-site positions P1-P5 are indicated. (d) Mutational analyses of the binding of Ulp1p to Kap60p. Immobilized 6 μg GST (lane 1) or 2.4 μg GST-Ulp1p (residues 150-172; lane 2, wild-type; lane 3, K155A mutant; lane 4, K168A mutant; lane 5, K155A/K168A mutant) was incubated with 18 μg ΔIBB Kap60p.

Fig. 5. GST pull-down assays of the assembly and disassembly of the yeast Kap95p-Kap60p-Ulp1p complex and a ternary complex formed by mammalian importin-β1, importin-α1, and SENP2. (a) Immobilized 6 μg GST (lane 1) or 2.4 μg GST-Ulp1p (residues 150-172, lane 2) was incubated with 20 μg Kap95p and 18 μg Kap60p. To assay disassembly of the Kap95p-Kap60p-Ulp1p complex (lanes 3-6), immobilized 2.4 μg GST-Ulp1p (residues 150-172) was incubated with 20 μg Kap95p and 18 μg Kap60p, unbound material washed away, and the beads were incubated with either 80 μg Gsp1p alone (lane 3, Gsp1p-GDP; lane 4, Gsp1p-GTP) or 20 μg Cse1p together with 80 μg Gsp1p (lane 5, Gsp1p-GDP; lane 6, Gsp1p-GTP). (b) Immobilized 6 μg GST (lanes 1) or 21 μg GST-SENP2 (residues 1-63)-importin-α1 complex (lane 6) was incubated with 15 μg importin-β1. To assay disassembly of the importin-β1-importin-α1-SENP2 complex, immobilized 6 μg GST (lanes 2-5) or 21 μg GST-SENP2 (residues 1-63)-importin-α1 complex (lanes 7-10) was incubated with 15 μg importin-β1, unbound material washed away, and the beads were incubated with either 25 μg Ran alone (lanes 2 and 7, Ran-GDP; lanes 3 and 8, Ran-GTP) or 25 μg Exportin-2 together with 25 μg Ran (lanes 4 and 9, Ran-GDP; lanes 5 and 10,

Ran-GTP). (c) Immobilized 6 μg GST (lane 1) or 13 μg GST-Ulp1p (residues 150-340, lane 2) was incubated with 20 μg Kap95p and 18 μg Kap60p. To assay disassembly of the Kap95p-Kap60p-Ulp1p complex (lanes 3-6), immobilized 13 μg GST-Ulp1p (residues 150-340) was incubated with 20 μg Kap95p and 18 μg Kap60p, unbound material washed away, and the beads were incubated with either 50 μg Gsp1p alone (lane 3, Gsp1p-GDP; lane 4, Gsp1p-GTP) or 20 μg Cse1p together with 50 μg Gsp1p (lane 5, Gsp1p-GDP; lane 6, Gsp1p-GTP). (d) Immobilized 6 μg GST (lane 1) or 20 μg GST-Ulp1p (residues 150-340; lanes 2-4) was incubated with 20 μg Kap95p alone (lanes 1 and 2) or 20 μg Kap95p together with 10 μg Gsp1p (lane 3, Gsp1p-GDP; lane 4, Gsp1p-GTP). (e) Immobilized 20 μg GST-Ulp1p (residues 150-340) was incubated with 20 μg Kap95p alone (lane 1), or 20 μg Kap95p together with 20 μg IBB-GFP (lane 2) or 20 μg GFP (lane 3). As negative controls, immobilized 20 μg GST-Ulp1p (residues 150-340) was incubated with 20 μg IBB-GFP alone (lane 4) or 20 μg GFP alone (lane 5).

Table 1 Crystallographic statistics.

Crystal	Kap121p (Δ80-90)-Ulp1p (1-150) complex	Kap60p (88-510)-Ulp1p (150-340) complex	Kap60p (88-510)-Ulp1p (150-172) complex
Data collection			
X-ray source	SPring-8 BL41XU	Photon Factory BL-1A	Photon Factory BL-17A
Wavelength (Å)	1.0	1.1	0.98
Space group	$P2_12_12_1$	$P1$	$P2_12_12_1$
Unit cell dimensions			
a, b, c (Å)	76.83, 124.71, 130.00	52.61, 63.54, 80.91	54.57, 77.48, 114.59
α, β, γ (°)	90.0, 90.0, 90.0	106.09, 107.72, 90.50	90.0, 90.0, 90.0
Resolution range (Å)[a]	36.71 - 2.80 (2.95 - 2.80)	30.37 - 2.50 (2.60 - 2.50)	49.27 - 2.20 (2.27 - 2.20)
$R_{merge.}$ (%)[a]	16.7 (72.8)	5.0 (16.3)	14.6 (78.7)
Mean $I/\sigma(I)$[a]	8.4 (2.9)	5.9 (3.0)	9.9 (2.9)
Mean *I* half-set correlation CC(1/2)[a]	0.995 (0.778)	0.995 (0.956)	0.995 (0.777)
Completeness (%)[a]	100.0 (100.0)	90.5 (91.0)	100.0 (100.0)
Multiplicity[a]	7.1 (7.2)	1.6 (1.7)	5.9 (6.1)
No. of reflections[a]	224445 (32662)	47966 (5757)	149220 (13112)
No. of unique reflections[a]	31520 (4556)	29881 (3417)	25386 (2165)
Refinement			
Resolution range (Å)	36.71 - 2.80	27.03 - 2.50	49.27 – 2.20
R_{work} / R_{free} (%)	19.8 / 24.1	21.4 / 24.7	20.2 / 22.8
No. of atoms			
Protein	7988	6667	3412
Water	0	85	220
No. of amino acids	1032	866	437
Mean *B* factor (Å^2)	59.4	40.5	32.4
R.m.s. deviation from ideality			
Bond lengths (Å)	0.005	0.003	0.003
Bond angles (°)	0.889	0.822	0.738
Protein geometry[b]			
Rotamer outliers (%)	0.8	0.6	0.3
Ramachandran outliers (%)	0.0	0.0	0.0
Ramachandran favored (%)	97.8	98.0	97.7
Cβ deviations > 0.25 Å (%)	0.0	0.0	0.0
Residues with bad bonds (%)	0.0	0.0	0.0
Residues with bad angles (%)	0.0	0.0	0.0
MolProbity score (percentile)	1.63 (100)	1.54 (99)	1.54 (98)
PDB code	5H2V	5H2W	5H2X

[a] Values in parentheses are for the highest resolution shell.
[b] MolProbity [31] was used to analyze the structures.

Figure 1

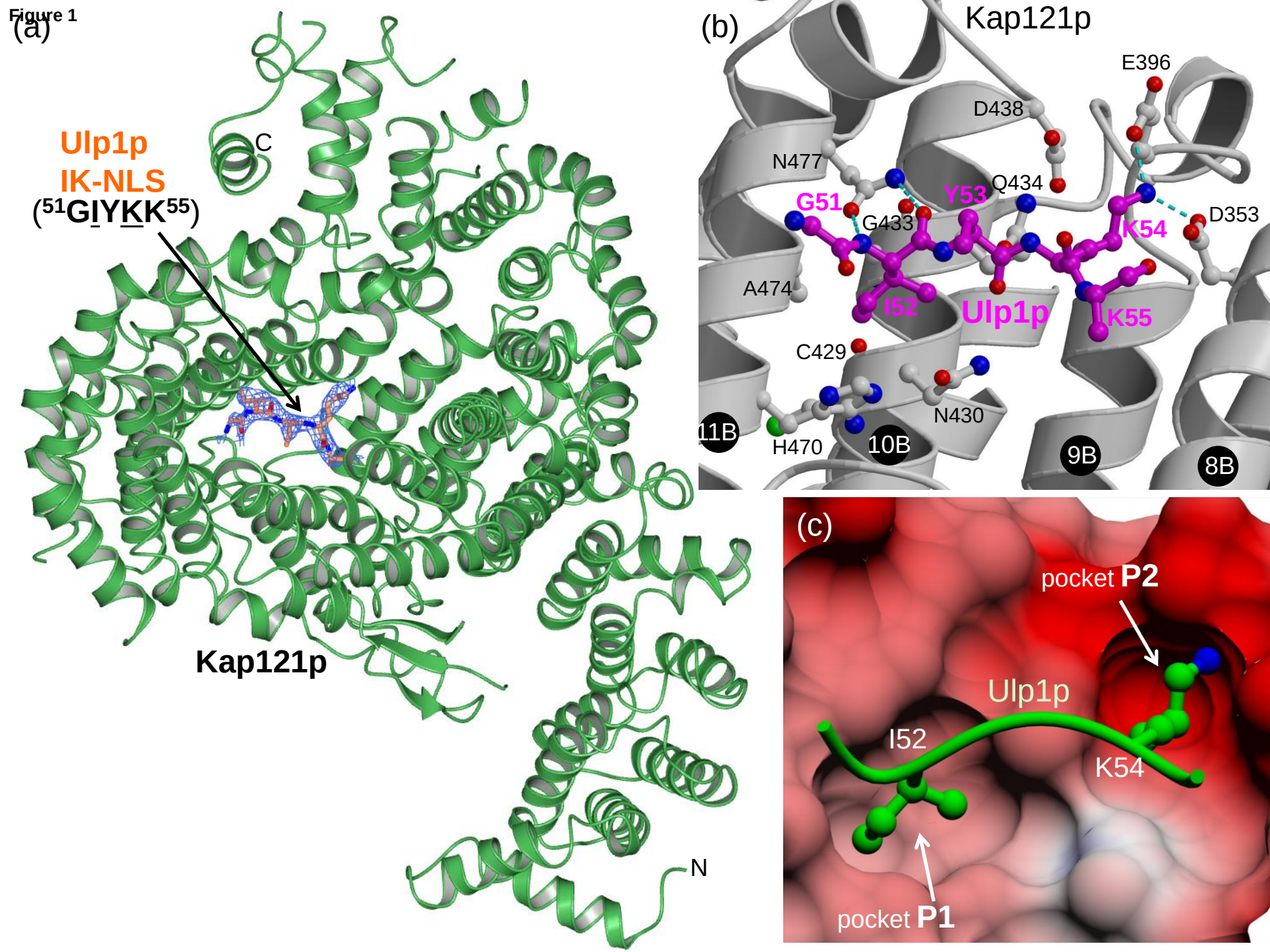
(a)
Ulp1p
IK-NLS
(51GIYKK55)
C
Kap121p
N
(b)
Kap121p
E396
D438
N477
Q434
G51
Y53
G433
K54
D353
A474
I52
Ulp1p
K55
C429
N430
H470
10B
9B
8B
(c)
pocket P2
Ulp1p
I52
K54
pocket P1

Figure 2

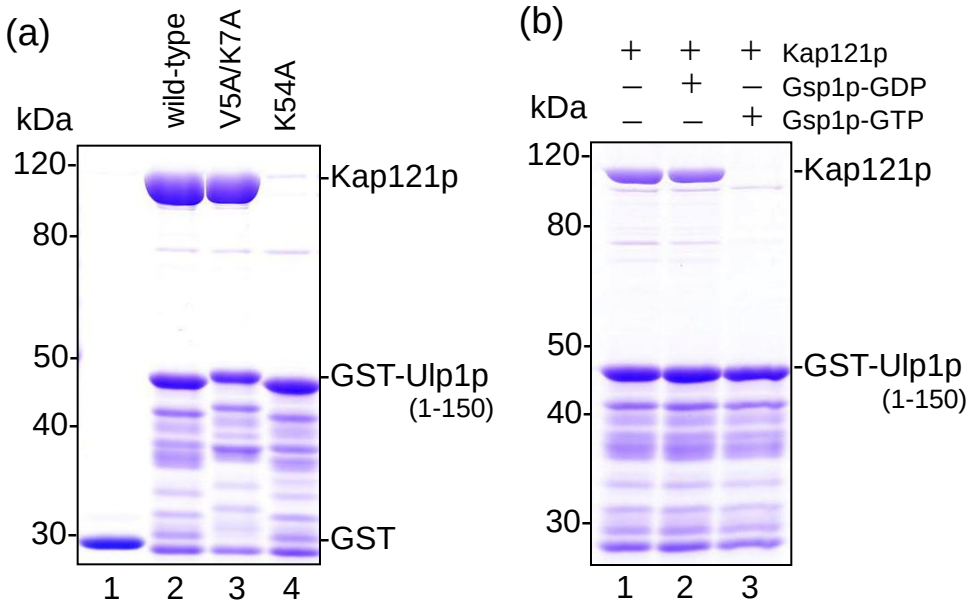
(a)
wild-type
V5A/K7A
K54A
kDa
120
80
50
40
30
Kap121p
GST-Ulp1p
(1-150)
GST
1
2
3
4
(b)
+ + + Kap121p
– + – Gsp1p-GDP
– – + Gsp1p-GTP
kDa
120
80
50
40
30
Kap121p
GST-Ulp1p
(1-150)
1
2
3

Figure 3

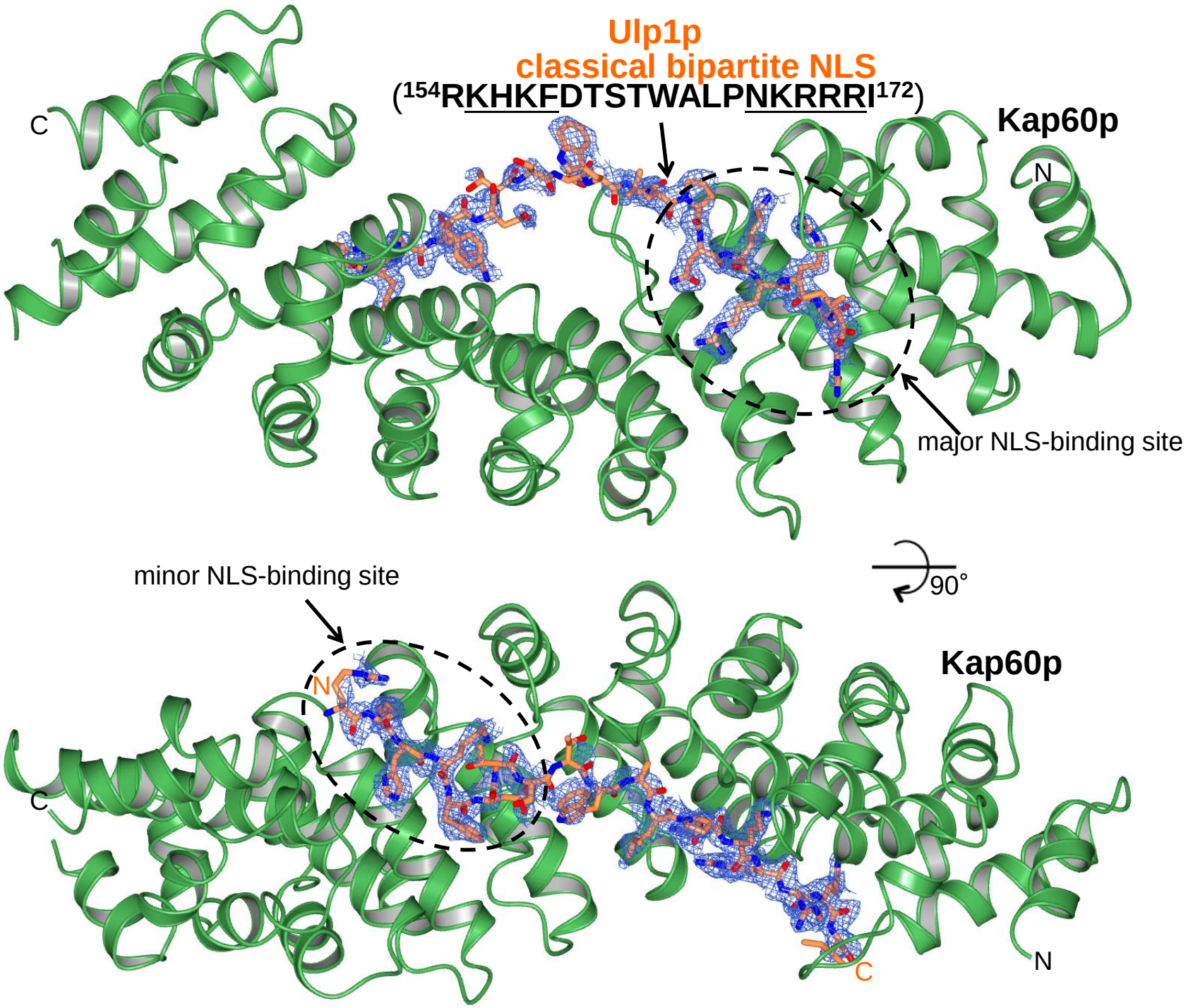
Ulp1p
classical bipartite NLS
(154RKHKFDTSTWALPNKRRRI172)
Kap60p
C
N
major NLS-binding site
minor NLS-binding site
90°
Kap60p
N
C
C
N

Figure 4

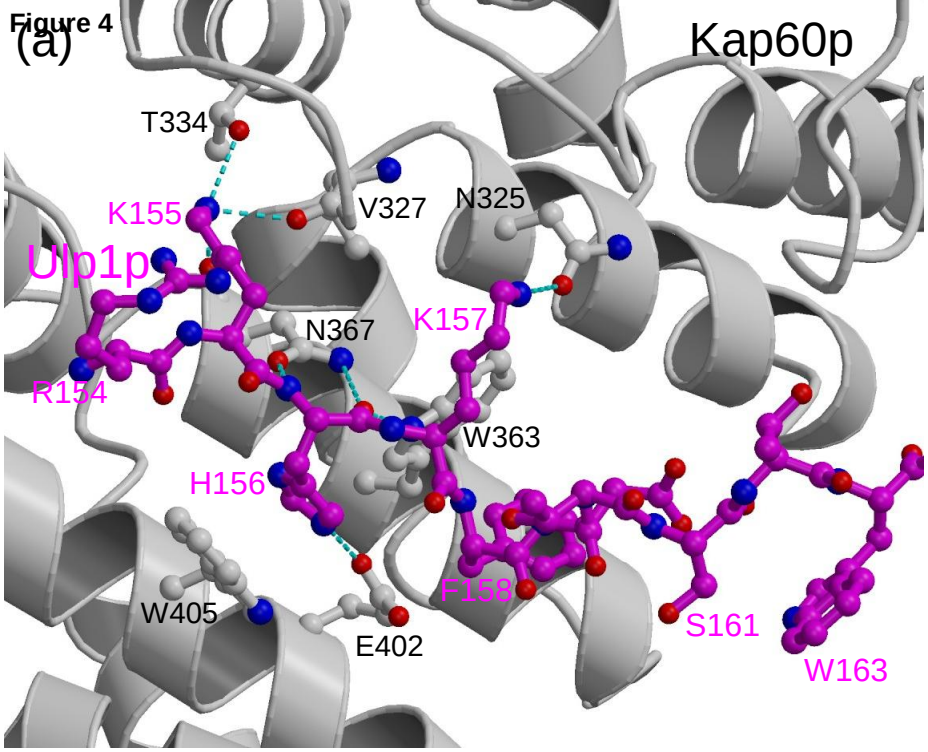
(a)
Kap60p
Ulp1p
T334
K155
V327
N325
N367
K157
R154
W363
H156
W405
F158
E402
S161
W163

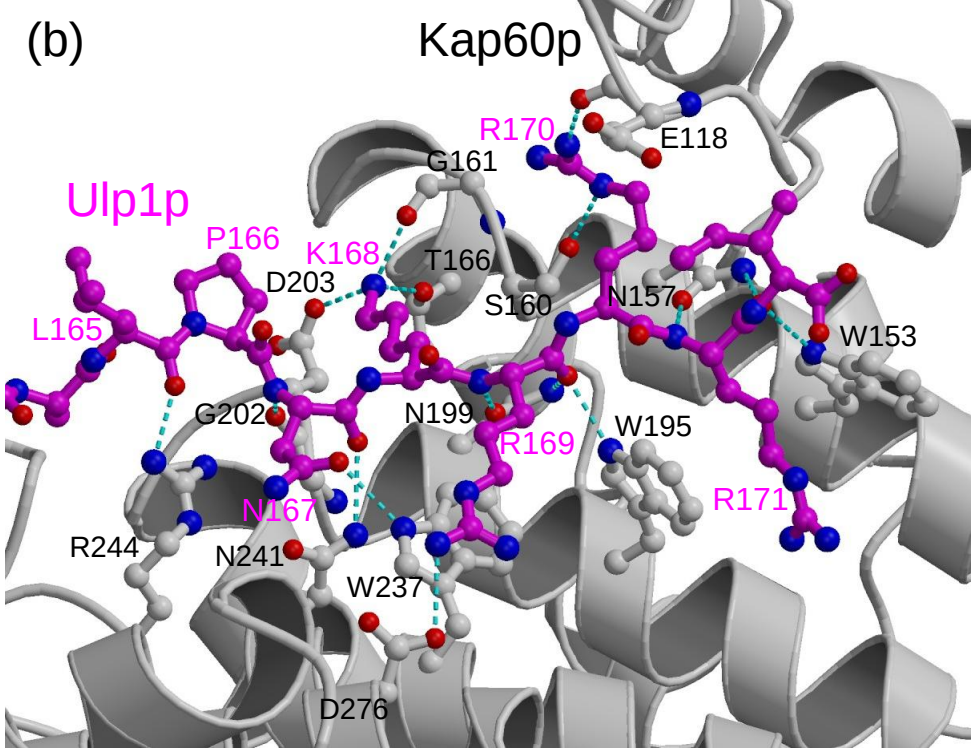
(b)
Kap60p
Ulp1p
R170
E118
G161
P166
K168
T166
D203
S160
N157
L165
W153
G202
N199
W195
R169
R171
N167
R244
N241
W237
D276

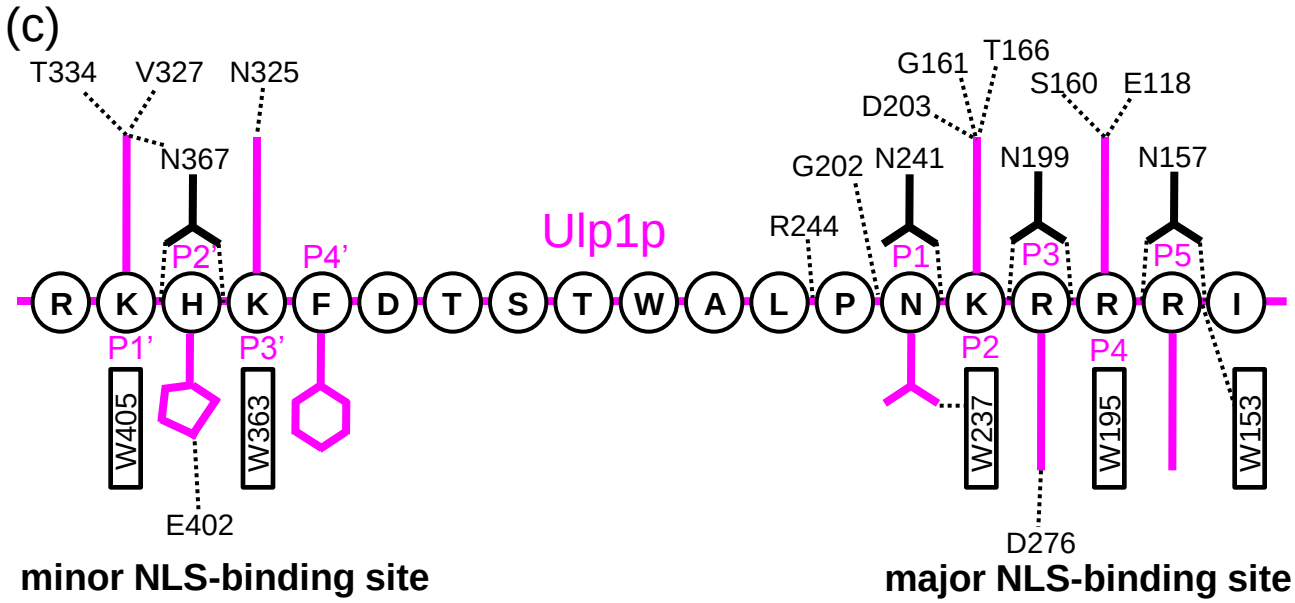
(c)
T334
V327
N325
N367
P2
P4'
Ulp1p
P1'
P3'
R K H K F D T S T W A L P N K R R R I
W405
W363
E402
G161
T166
D203
S160
E118
G202
N241
N199
N157
R244
P1
P3
P5
P2
P4
W237
W195
W153
D276
minor NLS-binding site
major NLS-binding site

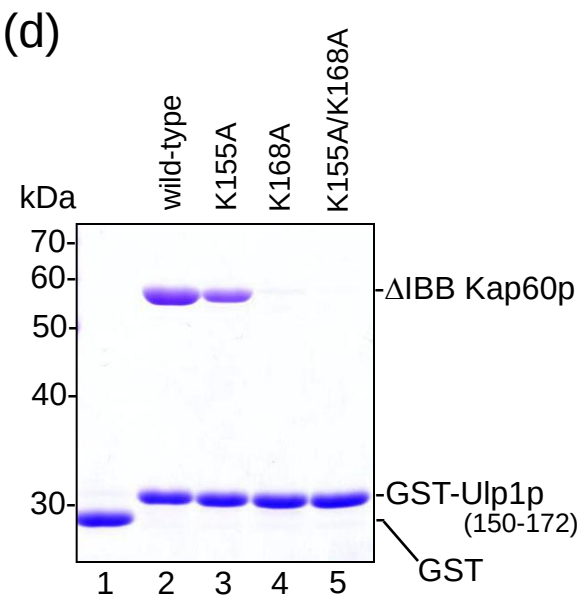
(d)
kDa
wild-type
K155A
K168A
K155A/K168A
70
60
50
40
30
ΔIBB Kap60p
GST-Ulp1p
(150-172)
GST
1
2
3
4
5

Figure 5

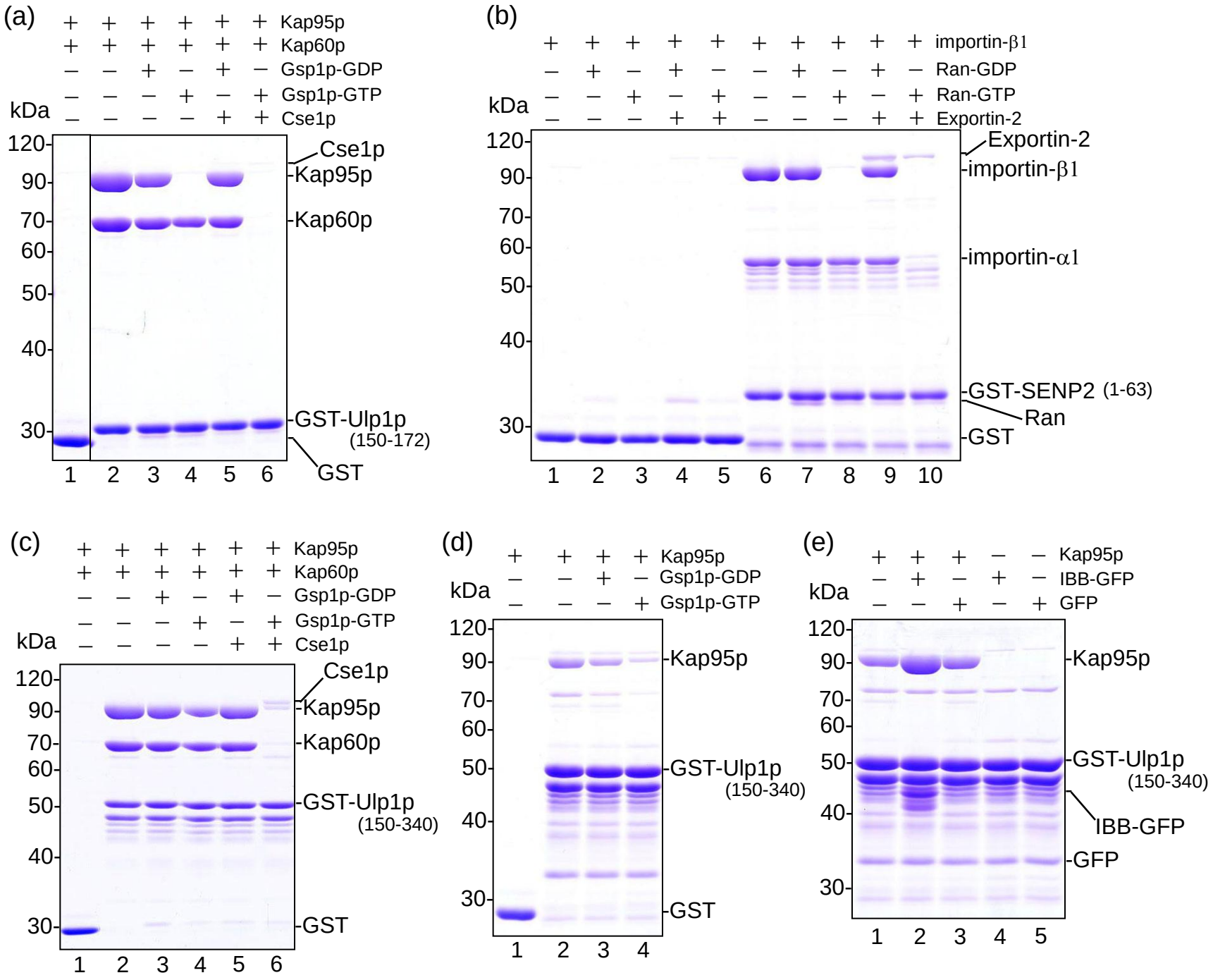
(a)
Kap95p
Kap60p
Gsp1p-GDP
Gsp1p-GTP
Cse1p
kDa
120
90
70
60
50
40
30
Cse1p
Kap95p
Kap60p
GST-Ulp1p
(150-172)
GST
1 2 3 4 5 6
(b)
importin-β1
Ran-GDP
Ran-GTP
Exportin-2
kDa
120
90
70
60
50
40
30
Exportin-2
importin-β1
importin-α1
GST-SENP2 (1-63)
Ran
GST
1 2 3 4 5 6 7 8 9 10
(c)
Kap95p
Kap60p
Gsp1p-GDP
Gsp1p-GTP
Cse1p
kDa
120
90
70
60
50
40
30
Cse1p
Kap95p
Kap60p
GST-Ulp1p
(150-340)
GST
1 2 3 4 5 6
(d)
Kap95p
Gsp1p-GDP
Gsp1p-GTP
kDa
120
90
70
60
50
40
30
Kap95p
GST-Ulp1p
(150-340)
GST
1 2 3 4
(e)
Kap95p
IBB-GFP
GFP
kDa
120
90
70
60
50
40
30
Kap95p
GST-Ulp1p
(150-340)
IBB-GFP
GFP
1 2 3 4 5

Supplementary Information

Structures of the karyopherins Kap121p and Kap60p bound to the nuclear pore targeting domain of the SUMO protease Ulp1p

Hidemi Hirano, Junya Kobayashi, and Yoshiyuki Matsuura

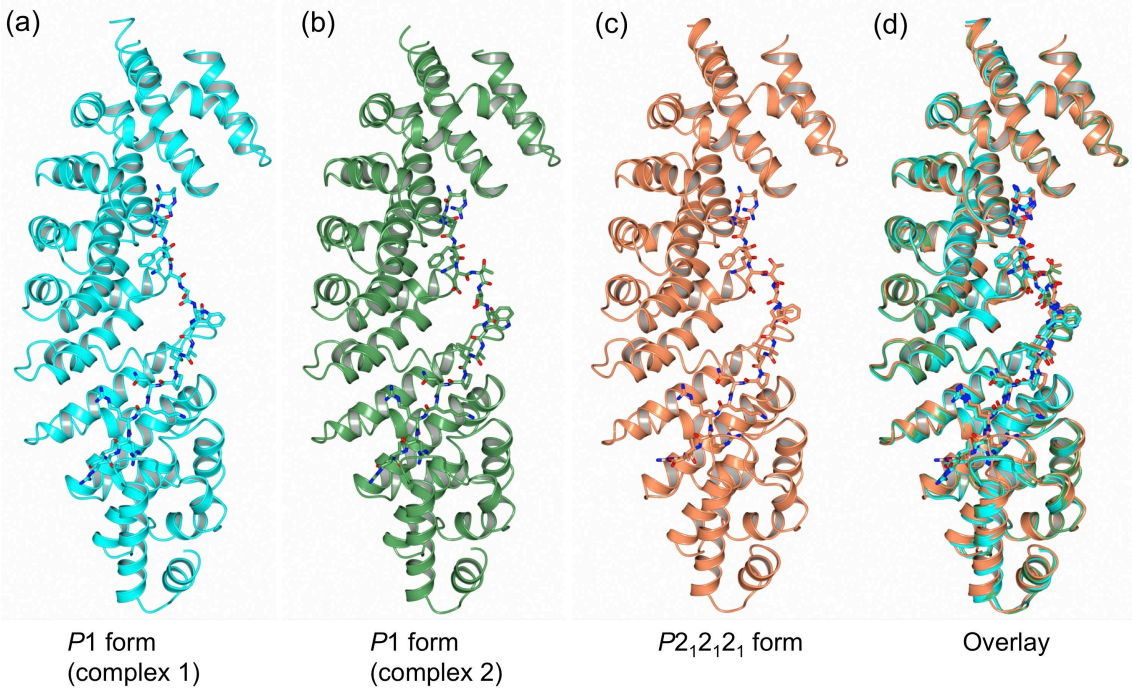

Fig. S1 Comparison of the crystal structures of the complex formed between Kap60p (ribbon model) and Ulp1p (stick model) in different crystal forms. (a, b) Two complexes in the asymmetric unit in the *P*1 crystal form (PDB code, 5H2W). (c) Structure of Kap60p -Ulp1p complex in the $P2_12_12_1$ crystal form (PDB code, 5H2X). (d) Overlay of the crystal structures shown in (a), (b), and (c).